3-3 Cloud Observation with CRL Airborne Cloud Radar (SPIDER)

HORIE Hiroaki, KUROIWA Hiroshi, and OHNO Yuichi

Cloud plays an important role of the transmission of radiation energy, but it was still remains with uncertainty. It is expected to observe three-dimensional distribution of cloud. Although it is difficult with usual weather radar, Communications Research Laboratory developed an Airborne Cloud Profiling Radar (SPIDER). Its sensitivity is -35 dBZ at 5 km range. In this paper, observation theory and method are discussed. Effectiveness of cloud profiling radar is explained with cloud data, which was obtained with airborne measurement.

1 Introduction

Clouds are the key to understanding the greenhouse effect and global warming. Clouds produce rainfall and play an important role in the transmission of radiation energy on the Earth, but it was still remains with uncertainty. In particular, the vertical distribution of clouds significantly affects the heating and cooling of the atmosphere. Measurement of the three-dimensional distribution of clouds[1] is thus required for more precise estimates of the global radiation budget.

It is difficult to measure clouds with conventional precipitation radar using microwaves because microwaves have wavelengths longer than the diameter of cloud particles; indeed, cloud particles are about 1/100 the size of raindrops. Therefore, if the wavelength of the radar is shortened, the scattering coefficient from cloud particles will be larger, resulting in an eventual enhancement of detection sensitivity. Current cloud observation radar employs radio waves of 35 GHz (wavelengths of 8 mm) and 95 GHz (wavelengths of 3 mm) bands. While the 95-GHz radar does not achieve high transmission power relative to the 35-GHz radar, it does have the advantage of being able to be incorporated into a smaller system, rendering it suitable for aircraft and satellite applications. The Communications Research Laboratory has been developing a millimeter airborne cloud radar system using 95 GHz frequency for cloud measurement (referred to as SPIDER[2]) since 1995. This radar system, detachable from the airplane, can also be used on the ground with a special pedestal. SPIDER is a multi-parameter radar system developed to explore a variety of possibilities for cloud remote sensing, and capable of transmitting or receiving dual orthogonal polarized signals, and detecting Doppler velocity. It has multiple measurement modes that may be customized according to the specific purpose of measurement. The antenna can scan within the angular ranges of 95 degrees on the left side (from the nadir direction) and 40 degrees on the right side (on a plane perpendicular to the track direction of the aircrafts). No other airborne 95-GHz cloud radar system is equipped with such antenna-scanning functions, in this time.

It is desired for cloud observation with cloud radar to obtain the vertical distribution of water and ice content in clouds, and size distribution of cloud particles. The Z factor in two orthogonal polarization, Doppler velocity and the FFT spectrum can be measured by

SPIDER. These measurement parameters may be combined to obtain data with respect to the three-dimensional distribution of clouds, estimate altitudes of the tops and bottoms of clouds, distinguish rain from clouds, identify cloud composition (e.g., water or ice), determine particle-size distribution, estimate the ice and water content in clouds, and perform correction for propagation loss and horizontal/vertical wind-speed components. If the cloud radar alone proves insufficient for a specific investigation, other sensors may be used in combination with the radar. Table 1 lists major examples of measurement applications conducted to date by SPIDER. Although there was a period during which the system did not work well, in recent years it has worked normally. In particular, the radar system was continuously operational for more than 2000 hours in MIRAI experiment (SPIDER was installed with research vessel, named MIRAI) from September to December 2001. Such a long period of operation was not reported other.

This paper describes the principles of cloud measurement and the capabilities of SPIDER, and also discusses its operational parameters. Then the result of recent airborne experiment is shown.

2 Principles of Cloud Measurement

2.1 Radar Equations

Such hydrometeors as rain and cloud particles (spread randomly in three dimensions) measured with a radar system having a narrow antenna-beam pattern are typically expressed by radar equation[3] below.

$$P_r = \frac{1}{\pi^2 2^{10} \ln 2} \frac{P_t G^2 \lambda^2 h \theta^2}{r^2 L} \eta \cdot 10^{-0.2 \int_0^r k dr} \qquad (1)$$

where P_r is the received power (mW), P_t the transmitted power (mW), G the antenna gain (dimensionless), the wavelength of the radio wave (m), h the pulse width (m), is the half-width of antenna beam (radian), r the distance from radar (m), the scattering cross-section (1/m) of hydrometeors per unit volume, L the system loss, $k = k_{wv} + k_{cl}$ the attenuation coefficient (dB/km), k_{wv} the attenuation caused by oxygen and water vapor in the atmosphere (dB/km)[4], and k_{cl} the attenuation caused by water and ice particles in the cloud (dB/km)[5]. Then, when the hydrometeors are much smaller than the wavelength of the employed radio wave, Rayleigh scattering can be assumed then the radar-scattering cross-section ( ) is given by:

$$\eta = \frac{\pi^5 |K|^2}{\lambda^4} 10^{-18} Z \qquad (2)$$

where $K = (m^2 - 1)/(m^2 + 2)$:the dielectric constant (m is a complex refractive index) and Z the radar reflectivity factor (mm^6/m^3). The radar reflectivity factor, Z, is defined by:

$$Z = \int N(D) D^6 dD \qquad (3)$$

where D is the particle diameter (mm) and N (D) the number of particles of diameter D per unit volume (m^3).

The radar reflectivity factor is called the Z factor, a quantity that eliminates terms related to wavelength from the scattering cross-sec-

Table 1 Summary of measurements using SPIDER

Time period	Measurement Platform	Content
January 1998	airplane	test flight after completion
March 1998	airplane	first measurement (failed)
June 1999	airplane	mesoscale project (failed)
February 2000	ground (CRL Kashima)	synchronization with B200 (particle probe)
February 2000	airplane	failed due to pressure leak
Sept. to Dec.2000	ground (CRL Kashima)	synergy experiment with lidar and radiometer
January 2001	airplane	synchronization with B200 (CAMPR) in mesoscale project
February 2001	airplane	synchronization with B200 (particle probe)
March 2001	ground (CRL Kashima)	synchronization with B200 (particle probe)
May 2001	ship	on board the measurement ship MIRAI
Sept. to Dec. 2001	ship	on board the measurement ship MIRAI
February 2002	airplane	mesoscale project (cooporative), sea-surface measurement (performed by CRL alone)

tion, leaving only those terms relating to hydrometeor particles. The Z factor is the typical variable in radar measurement. A logarithm of the Z factor (in dBZ) is often used. Equations (2) and (3) indicate that the scattering cross-section is proportional to the sixth power of particle size and inversely proportional to the fourth power of wavelength. While an average diameter in raindrops is 2 mm, the typical diameter of cloud particles is 0.01 mm, or at least 100 times smaller. Thus the radar's per-particle detection sensitivity declines by at least 10 to the 12th power (120 dB) within a cloud relative to its sensitivity in rain. Meanwhile, equation (2) indicates that shorter wavelengths will result in higher sensitivity. Indeed, compared with the 10-GHz band (X-band; wavelength of 3 cm), sensitivity can be improved by as much as 22 dB in the 35-GHz band (Ka-band; wavelength of 8 mm) and 39 dB in the 95-GHz band (W-band; wavelength of 3 mm). Equation (1) also indicates that the received power is inversely proportional to the square of the scattering range (which is far from radar). Thus, the closer the measured object is to the radar, the easier it is to measure scattering, even given the same Z factor. For example, sensitivity rises by as much as 14 dB (or 25 times higher) when the scattering range is shortened from 5 km to 1 km. Therefore, it is advantageous to perform airborne measurement.

2.2 Measurement Parameters

The polarimetric radar provides such variables as the Z factor of the horizontal and vertical polarized signals, the difference in the Z factor between both polarized signals (Z_{DR}: Differential Reflectivity factor) and the linear depolarization ratio (L_{DR})[3]. Via pulse-pair processing, Doppler velocity, spectrum width, and differential phase (ϕ_{DP}), and the correlation coefficient between the horizontal and vertical signals (ρ_{HV} (0)) can be obtained in addition. From FFT processing instead of pulse-pair processing, Doppler spectrum can be obtained. The vertical component of Doppler velocity may be provide useful data

in distinguishing between cloud and rain, while L_{DR}, Z_{DR}, and attenuation in Z, and ϕ_{DP} and ρ_{HV} (0) may provide useful information to help distinguish between water clouds and ice clouds.

Conversely, there is no one-to-one relationship between the Z factor (provided by radar) and liquid water content (LWC) or ice water content (IWC). M (g/m³), which is LWC in such water clouds as cumulus clouds and IWC in such ice clouds as cirrus clouds, is expressed by the following equation:

$$M = \frac{\pi\rho}{6\cdot10^6}\int_0^\infty D^3 N(D)dD \qquad (4)$$

where ρ is the density of water or ice (g/m³). The reflectivity factor (Z) is a quantity proportional to the sixth power of D, while M is proportional to the third power of D. Thus, the particle-size distribution (N (D)) must be identified for consistency between Z and M. In several examples[6][7], Z and M are related based on a size distribution determined experimentally. This relationship, however, greatly depends on whether the cloud consists of water or ice and even on other factors. Thus, other methods, such as the calculation of particle-size distribution based on the differences in scattering mechanisms between radar and lidar for ice clouds, and calculation of the liquid water content profile based on a boundary condition with respect to the integral water content provided by the microwave radiometer, had been proposed [8][9][10].

2.3 Instrument and its Performance

The airborne cloud radar[2] developed by the Communications Research Laboratory (CRL) for cloud measurement consists of a radar pod housing the RF unit and antenna on the outside of the aircraft, and the IF unit, and data processing and recording unit inside the aircraft. Fig.1 illustrates the airborne cloud radar aboard the airplane; Fig.2 is a photo of the radar pod opened to expose the installed antenna. The antenna is closed in the radar pod during takeoff. Table 2 lists the major system parameters of SPIDER. Reference[2]

The radar pod can be seen on the left side and the data processor is installed inside the airplane.

The RF unit and antenna are housed in the radar pod. The antenna scans the vertical plane cross-track direction.

Table2 *SPIDER system parameters*

Frequency (wavelength)	95.040 GHz (3.16mm)
Antenna aperture	40 cm
Antenna beam width	0.6 degrees
Antenna gain	49.4 dBi
EIK transmitting power	1,600 W
Maximum duty cycle	1%
Pulse width	0.25, 0.5, 1.0, 2.0 μs
Pulse repetition interval	arbitrary value equal to the duty ratio or less
Pulse sequence	selectable from among 1, 4, and 6
Receiver NF	4.5 dB (LNA)
Receiver dynamic range	75 dB
Transmitting polarization	linear, horizontal/vertical switchable for each pulse
Receiving polarization	linear, horizontal/vertical, simultaneous receiving
Data processing	real-time processing, FFT or pulse-pair mode
Antenna scanning	-40 degrees to +95 degrees (0 degrees: nadir)
Flight-altitude	maximum 13 km
Cruising speed	100 to 250 m/s

goes into further detail. The system features the unprecedented capability of scanning the antenna in the plane perpendicular to the track direction of the airplane. Thus, it is possible to measure a wide area beneath the airplane during flight. SPIDER is equipped with two channels of receiver for the measurement of orthogonal linear polarized signals. As we have discussed, when the antenna is deployed (at 90 degrees), the orientation providing vertical polarization is V polarization and the V receiver receives the V-polarized signals; similarly, the orientation providing horizontal polarization is called H polarization and the H receiver receives the H-polarized signals.

These receivers have been designed to have a sensitivity of -30 dBZ for the Z factor. According to reference[11], if the sensitivity to measure cloud is better than -30 dBZ in Z factor, the radar can measure as much as 84 % of the clouds relating to radiation budget in the middle-latitude area. Another report[1] suggests that as much as 99 % of clouds will be measurable on the same condition. The goal thus became to develop a new radar system to attain a sensitivity of -30 dBZ at 5 km range for normal operational parameters.

In general, the average received power (P_r) when the signal phase is random, such as with radio waves scattered by hydrometeor particles, is given by equation[8] below,

$$\overline{P_r} = \overline{P_s} + \overline{P_n} \qquad (5)$$

where, P_s is the signal power (scattering power returned from particles) and P_n is the noise power. Meanwhile, the true signal power can be obtained by subtracting noise power from received power. The noise power (P_n) can be estimated from the characteristics of the receiver as follows:

$$P_n = kT_{rec}B \qquad (6)$$

where k is the Boltsmann constant (1.38×10^{-23} J/K), Trec the equivalent noise temperature (K) of the receiver, and B the receiver bandwidth (Hz). The equivalent noise temperature of the receiver (T_{rec}) is expressed by the equation below,

$$T_{rec} = (L-1)T_0 + L(NF-1)T_p \qquad (7)$$

where NF is noise figure of the low-noise amplifier (LNA), L is waveguide loss between the antenna and LNA, T_0 (K) is the temperature of the antenna and waveguide, and T_p is the temperature of the receiver (LNA).

For SPIDER, waveguide loss L is about 4 dB and the receiver noise figure NF is 4.5 dB. Then, if Tp and T0 is assumed to 300 (K), the equivalent noise temperature becomes 1,823 K according to Equation (7). When 1-ms pulses are used in transmission, noise power is calculated to -102 dBm by Equation (6). Fig.3 shows the predicted received power with the Z factor as a parameter. Equation (5) indicates that received power will not become smaller than noise power even when there are no clouds in the sky.

S_n refers to signal to noise ratio (SNR), or the SN ratio, and is give by the equation below,

$$S_n = P_s / P_n \qquad (8)$$

Note that S_n is also described in dB in most cases. First, it supposes that the detection limit is determined by $S_n = 0$ dB when signal power is equal to noise power. Fig.3 also shows a diagram illustrating the detectable Z values. For example, Fig.3 indicates that the detection limit is about 5 km range when sensitivity is -30 dBZ. Meanwhile, the received power corresponding to -30 dBZ at a point 5 km range is -99 dBm. In this condition of the detection limit, the received power, which is 3 dB larger than the noise power, becomes the limit. If the noise power is subtracted, Z is detectable even when Sn is smaller than zero dB or noise power is larger than signal power. In case of scattering from hydrometeor particles, an appropriate number of pulses must be averaged. The detection limit is then based on a determination as to whether noise power can be deducted from the averaged power. For this purpose, we make use of the variance of averaged power. The variance of received power, (σ_{rdN}), and that of noise power (σ_{ndN}), are given by the equations below, with their
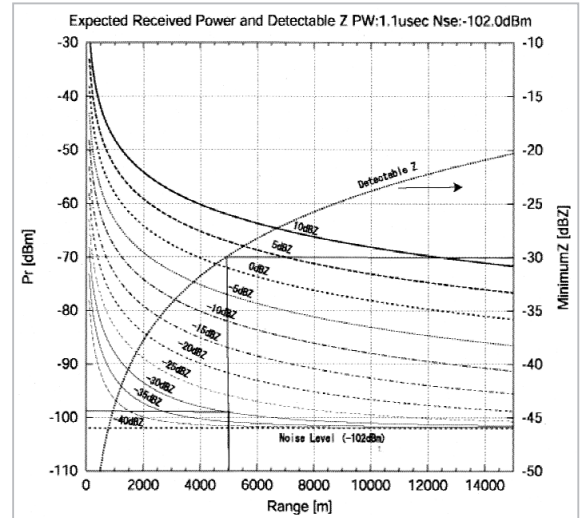

Fig.3 *Received power and minimum Z factor versus range from radar*

Received power is shown for each Z factor. As the radar equation (Equation1) indicates, the received power decreases with increasing range. The Z factor is plotted that provides a noise power equal to signal power. Refer to the right axis as well.

respective averaging numbers being N_r and N_n.

$$\sigma_{rdN} = \frac{\overline{P_s}}{\sqrt{N_r}}\left(1 + \frac{1}{S_n}\right) \qquad (9a)$$

$$\sigma_{ndN} = \frac{\overline{P_n}}{\sqrt{N_n}} \qquad (9b)$$

By using these equations and Equation (5) as well as those for variance, we come up with the equation below, which normalizes the variance (σ_s) of signal power with actual signal power (P_s).

$$\frac{\sigma_s}{P_s} = \sqrt{\frac{1}{N_r}\left(1 + \frac{1}{S_n}\right)^2 + \frac{1}{N_n}\left(\frac{1}{S_n}\right)^2} \qquad (10)$$

We summarize that signals are detectable if the variance of signal power after averaging is at least one-half the true signal power. Equation (10) provides a solution, assuming that the left side of the equation is equal to one-half. The S_n required for signal detection is determined by the integral values of signal and noise. The detectable S_n is determined by averaging number of signal and noise. Usually, the averaging number of noise is larger than that of signals to stabilize noise power. Fig.4 is the plot of S_n at detection limits with N as a parameter, with $N_n = N*N_r$. This figure
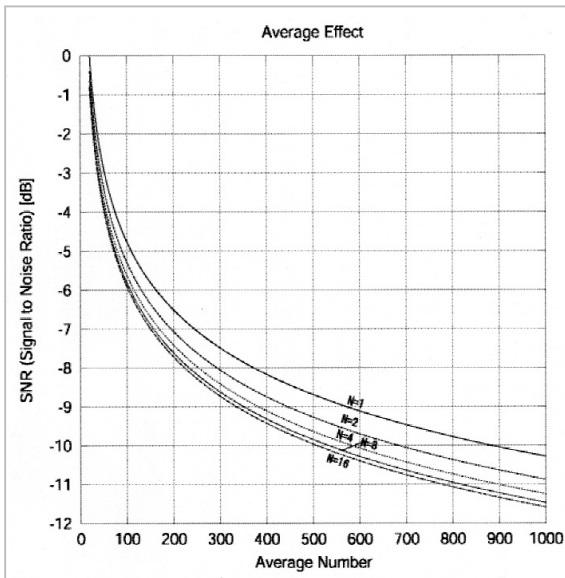
Fig.4 *Averaging number and Minimum detectable SN limit*

Plotted with a multiplier number of the sampling number of signal power for noise power. Refer to Equation 10.

shows that S_n at the detection limit is -5.8 dB when the averaging value (N_r) is 100 and the averaging value multiplier (N) of noise is 8. In the above example, clouds can be measured with a sensitivity of -35 dBZ in the 5-km range.

2.4 Discussion of Measurement Modes

The development of a measurement algorithm and various accompanying measures are considered for the study using SPIDER system. Accordingly, we have prepared three categories of measurement modes: (1) pulse-pair mode, (2) FFT mode, and (3) RAW data recording mode. Modes in the pulse-pair category include SPPMAG mode, which transmits one polarized pulse in one sequence, PPMAG4 mode, which transmits four polarized pulses in one sequence, and PPMAG6 mode, which transmits six polarized pulses in one sequence. Each pulse may consist either of an H-polarized signal or V-polarized signal, as desired. Since the two receivers are operative simultaneously, both copolar and cross-polar components can be obtained. Either the copolar or cross-polar component can be selected for pulse-pair processing. The FFT category, on the other hand, may be divided

into FFT mode and DPFFT mode. Both modes provide FFT data for the selected polarized signal during transmission. However, FFT mode only provides copolarized data, while DPFFT mode provides cross-polarized data in addition. In RAW data mode, the parameter settings are the same as those for PPMAG4 mode. The difference here is that this mode records the all-hit data as is, and acquires no averaging data. This mode is useful for comparing different analyses (such as FFT analysis and pulse-pair analysis) using the same data, and also for analysis using individual-pulse data.

In all the modes, pulse intervals can be set at an arbitrary value in 1-μ s blocks. All modes are limited by buffer memory size. This should be chosen for a given application. As listed in Table 3, there are maximum limits to integral of multiplier for the number of averaging N_{av}, number of range gate N_{rg}, number of multiplier for noise N_n, and FFT bins number N_{bin} in FFT mode. For example, in PPMAG6 mode, if pulses with 1 micro-sec width are transmitted and maximum range gate is 15 km using twice of over sampling, the upper limit of the averaging value is 32, assuming that the noise sample number is 8.

The characteristics of the major observation parameter are listed below.

Table 3 *Limitations on operational mode*

MODE	Equation	Number of limitation
SPPMAG	Nav*(Nrg+Nn+1)	53376
PPMGA4	Nav*(Nrg+Nn+1)	8896
PPMGA6	Nav*(Nrg+Nn+1)	5930
FFT	Nav*(Nrg+Nn+1)*Nbin	53376
DPFFT	Nav*(Nrg+Nn+1)*Nbin	35584
RAWDATA	Nav*(Nrg+Nn+1)	2048

(1) PPMAG4 mode, polarization: HHVV, Pulse Interval: 110, 110, 110, 550 (μ s)

This mode is useful for the measurement of LDR and ZDR. Copolar Doppler data is provided for both H and V-polarized signals. The longest pulse interval of 550 μ s, is useful in reducing the duty ratio and keeping coherent time for increasing independent samples.

Moreover, this long interval may be useful when reducing the data quantity (in accordance with the integral-value limit) over the course of an extended period of measurement.

(2) PPMAG4 mode, polarization: VHVV, Pulse Interval: 110, 110, 110, 550 (μs)

This mode is useful for measuring the correlation ($_{HV}$(0)) between polarized signals. Doppler data on the copolar H polarized signals is not provided through measurements in this mode.

(3) PPMAG4 mode, polarization: VHHH, Pulse Interval: 110, 110, 130, 550 (μs)

This mode includes staggered pulses. Staggered pulses work to make data correction easier by shifting the Doppler folding point by varying pulse intervals. For example, if the pulse intervals are 110 μs, the folding point lies at about 7.2 m/s, which is too small when Doppler data includes the aircraft-speed component and horizontal-wind-speed component.

(4) PPMAG6 mode, polarization: VHHVV, Pulse Interval: 110, 110, 130, 110, 110, 550 (μs)

This mode covers all modes (1)-(3) above. Due to the limitation of the data aquisition system buffer, the number of averaging cannot be made large.

Conversely, antenna scanning features three modes: (1) Pointing mode, (2) Scan mode, and (3) Step mode. These modes, dealing with various settings for operating time, may be combined in use. In most cases, pointing mode is employed to perform downward measurement from an aircraft, upward measurement from the ground, and lateral measurement for an in-cloud flight. Scan mode is employed to determine the three-dimensional distribution of clouds or clarify the dependence of sea-surface scattering upon an incident angle, which is used for data correction.

The antenna can be set to move at a speed of 30 deg./s, but the antenna angle data is provided at intervals of 30 m/s (at the shortest). If the antenna is set to move at the highest speed, it will move 0.9 degrees in 30 m/s—greater than the half-width of antenna beam (0.6 degrees). Thus the antenna is set to move

20 deg./s or slower. In addition, the speed of antenna movement should be determined with reference to the data-averaging time. In the frequently-used scan over the -30 to +30-degree range, for example, the speed of antenna movement is set at 10 deg./s.

3 Description of airborne measurement

—Measurement of cloud band and convergent cloud during cold winds—

The following describes a flight measurement conducted on February 11, 2002. This experiment was conducted in the WMO-02 (Winter Mesoscale Convective Systems Observations over the Japan Sea/2002), part of the core research for the evolutionary science and technology series entitled, "Studies on the Structure and Formation/Development Mechanisms of a Mesoscale Convective System" (led by Masanori Yoshizaki). Similar measurements were conducted in 2001 as well[1 2]. At first, comprehensive measurements employing a variety of measurement devices on the ground and ocean were scheduled. However, only airborne observation was actually performed as the aircraft condition required postponement. The aircraft, a Gulf Stream II, was equipped with a drop sonde, in-situ probe for direct observation of cloud particles, and microwave radiometer, in addition to cloud profiling radar.

On the day of the experiment, a relatively strong cold wind blew over the Japan Sea and a convergent cloud was generated. Fig.5 shows the visible image by the meteorological satellite HIMAWARI (GMS). This figure also shows the flight path, which was set to cross the convergent cloud. The aircraft flew along a latitude of 36.30 degrees North between a longitude of 133 degrees East and 136 degrees. The plane flew this course four times at different altitudes. Fig.6 is a schematic description of the measurements. Four different altitudes were selected because the meas-
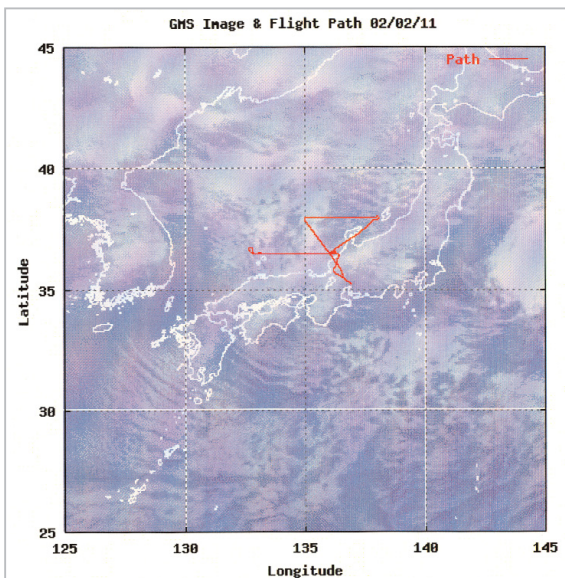
Fig.5 GMS Visible image of 14JST on February 11, 2002 (courtesy of Kochi University) and superimposed flight path

The flight path was set along latitude 36.30 degrees North between East longitude 133-136 degrees at four different altitudes.
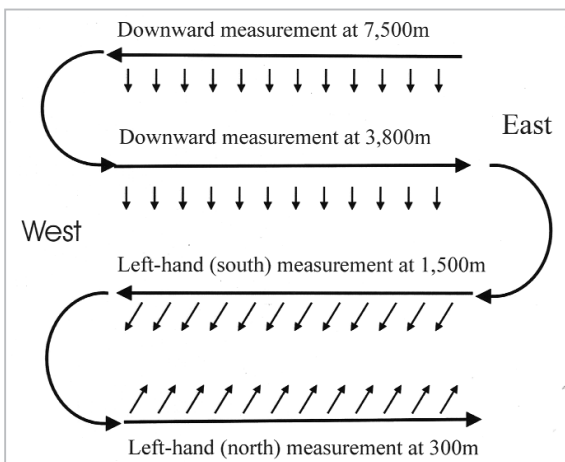

Fig.6 Schematic diagram of the flight path

A) Downward measurement in the east-west flight at 7,500 m
B) Downward measurement in the west-east flight at 3,800 m
C) Left-hand (south) measurement in the east-west flight at 1,500 m
D) Left-hand (north) measurement in the west-east flight at 300 m

urement devices aboard the airplane worked differently at different altitudes. First, radar observation was made from the sky above the cloud at an altitude of 7,500 m. In that experiment, a drop sonde was launched at the edge of the test course for sonde measurement. Second, measurement was performed at an altitude of 3,800 m near the top of the cloud. In the flight test at 1,500m, the plane flew into the cloud for in-situ measurement by probe. The radar antenna was moved horizontally to measure the cloud spread and horizontal velocity of cloud. The bottom of the cloud was located at an altitude of 300 m, and the radar antenna was deployed for measurement at this altitude. Fig.7 shows the Z-factor image obtained in this measurement. The horizontal- axis represents the horizontal distance corresponding to the latitude of Japan map, depicted at the bottom of the four diagrams, while the vertical axis represents distance from the radar and corresponds to the nadir direction in the flights at (A) 7,500 m and (B) 3,800 m. The red horizontal line in the figure is corresponding to sea surface. The images for this flight at (C) 1,500 m and (D) 300 m are the results of horizontal measurements toward to left from airplane. Specifically, the southern side was measured during the 1,500-m flight, while the northern side was measured during the 300-m flight. The flight altitude of the aircraft at lower altitudes was frequently disturbed by air turbulence. The 300-m flight shows strong echoes returned from far range. These are the results of scattering from the sea surface caused by airplane motion. Specific data correction related to airplane attitude was not made in this case.

The 7,500-m flight took a course headed west, while the 3,800-m flight took a course headed east. On the east side of the flight path, the aircraft took at least an hour to move to measurement at 3,800-m from the 7,500-m measurement altitude. The data of the measurements is plotted on the common latitude line. Referring to pictures (A) and (B), we can recognize that strong echoes were moved to east in (B), and weak echo, too. This movement of clouds over time is agreed with GMS image (data not shown).

One cell during the time period from 13:34 to 13:38 was picked up and showed the Z factor and Doppler velocity in Fig.8. The Z factor (Fig.8a) shows an echo reaching sea level at around 13:36. The white horizontal line at
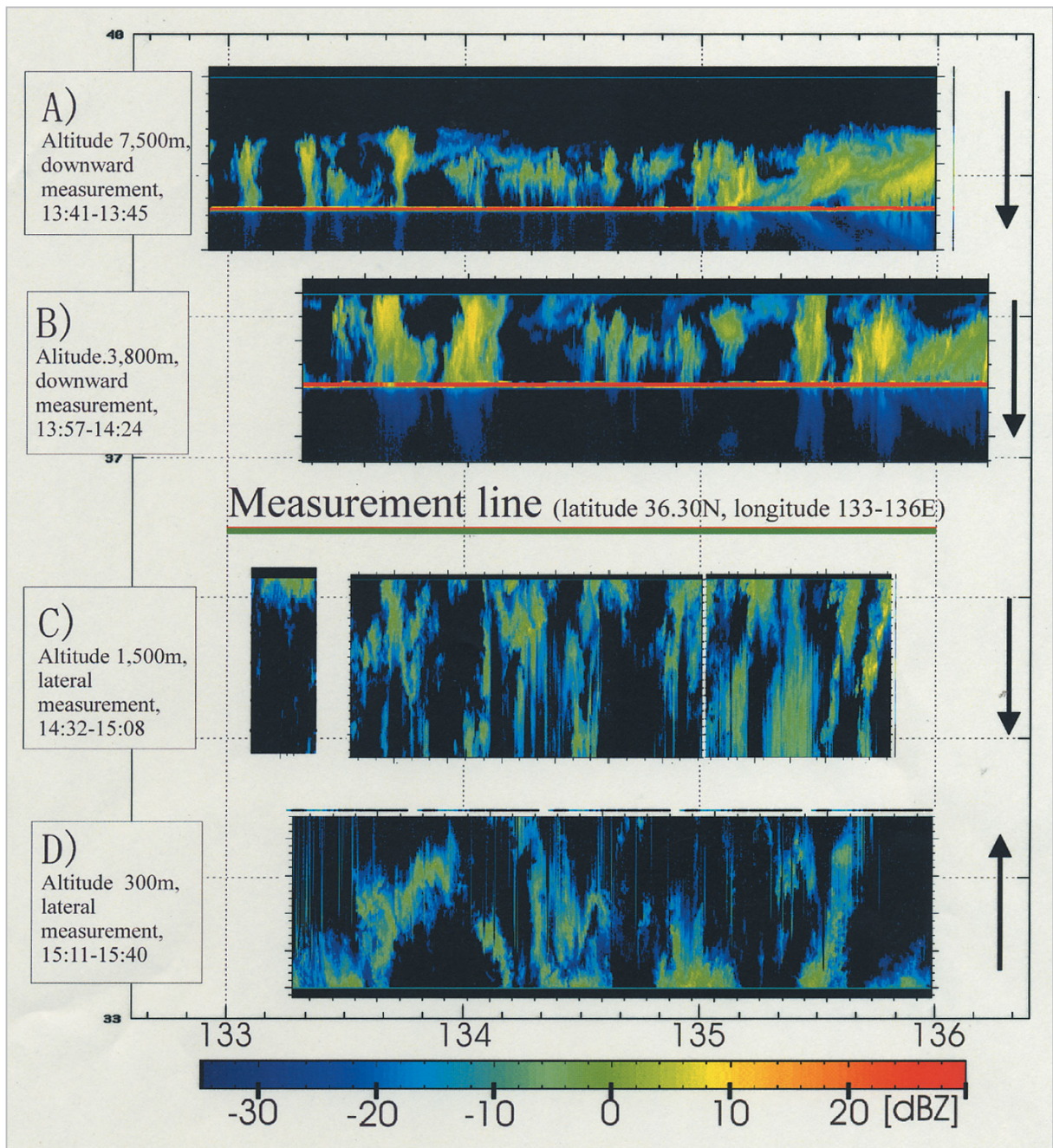
Fig.7 *Z factor measured in February 11 (2002)*

Data taken by PPMAG6 mode with a pulse width of 1 μs is averaged over every one second. Each graph corresponds to A-D in Fig.6. The averaging numbers are A) 528, B) 750, C) 300 and D) 360. The distance in the east-west direction is reduced to the bottom longitude. A) and B) are nadir measurements. The red line represents the sea surface. C) is the measurement of the south side of the measurement line (top line of the graph; the measurement range is 23 km). D) is the measurement of the north side of the measurement line (bottom line of the graph; the measurement range is 23 km).

around 7,500 m represents the sea surface. Because the scattering from the sea surface is larger than 25 dBZ converted to Z factor, it is shown in white color. Where smaller than 25 dBZ, the scattering is drawn in red. Accordingly, there are some red areas at approximate-ly 13:36. This is probably due to the fact that the signals were attenuated during propaga-tion. The echoes up to approximately 2 km above sea level are weaker than those seen at higher altitude. Clearly, the corresponding Doppler velocity (Fig.8b) are directed down-

ward. According to the equation of terminal speed, a large downward velocity implies a large particle size, which will result in a large Z factor. Thus the above attenuation may indicate that the radio waves were weakened during propagation. Fig.8b also shows an upward Doppler velocity that may indicate the existence of an upstream air turbulence in the upper layer of the cloud. It is possible to interpret particle behavior in the cloud by examining these results in detail. Comparing the radar data obtained above the cloud with the in-situ measurement data afterward, must be done with taking cloud movement into account. The measurement data taken by the deployed antenna will be analyzed from a polarimetric standpoint.
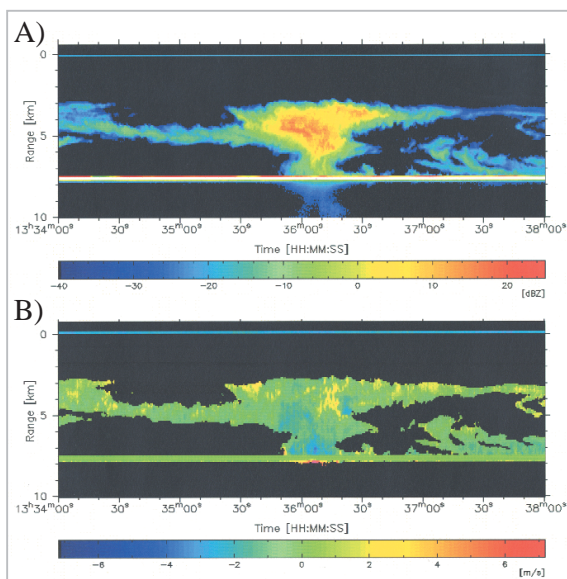

Fig.8 *Enlarged image of a cloud*

A) Z factor, B) Doppler velocity of the cloud measured during the time period between 13:34 to 13:38. This diagram is part of Fig.7A. The averaging time is 0.5 seconds, or 264 as the averaging number.

4 Conclusions

This paper has described the concept behind the development of an airborne cloud radar and its functions, along with its operational parameters. SPIDER shows a high degree of flexibility in measurement and allows a wide variety of measurements through variable settings of operational parameters, depending on the application. It has been used in diverse contexts, exhibiting the required sensitivity on the ground, at sea, and in the air, thus attracting a great deal of attention from domestic and overseas meteorologists.

This paper has explained the experimental data gathered in the Winter Mesoscale Convective Systems Observation project over the Japan Sea. We measured vertical cloud distribution over 300 km in horizontal, where a flight test performed twice on the same course measured cloud movement over time. By picking up the cloud cells for this analysis, it is possible to understand cloud behavior through estimates of the upstream and downstream velocities of clouds. Detailed analysis in this area awaits further investigation.

Acknowledgment

References

1 P. R. Brown, A. J. Illingworth, A. J. Heymsfield, G. M. McFarquhar, K. A. Browning, and M. Gosset, "The role of spaceborne millimeter-wave radar in the global monitoring of ice cloud", J. Appl. Meteor., Vol.34, pp. 2346-2366, 1995.

2 H. Horie, T. Iguchi, H. Hanado, H. Kuroiwa, H. Okamoto and H. Kumagai, IEICE Trans. Commun.,

Vol. E83-B, pp.2010-2020, No.9, Sep. 2000.

3 R. J. Doviak and D. S. Zrnic, "Doppler Radar and Weather Observation", 2nd Ed., Academic Press., 1993.

4 F. T. Ulaby, R. J. Moor and A. K. Fung, "Microwave Remote Sensing – active and passive – ", Artech House Inc., 1981.

5 R. Lhermitte, "Attenuation and scattering of millimeter wavelength radiation by clouds and precipitation", J. Atmos. Ocean. Technnol., Vol. 7, pp. 464-479, 1990.

6 H. Sauvageot and J. Omar, "Radar reflectivity of cumulus clouds", J. Atmos. Ocean. Technnol., Vol.4, pp. 264-272, 1987.

7 K. Sassen, "Ice cloud content from radar reflectivity", J. Climate Apllied Meteor., Vol.26, pp.1050-1053, 1987.

8 S. Y. Matrosov, A. J. Heymsfield, R.. Kropfli, B. E. Martner, R. F. Reinking, J. B. Snider, P. Piironen, and E. W. Eloranta, "Comparison of ice cloud parameters obtained by combined remote sensor retrievals and direct methods", J. Atmos. Ocean. Technol., Vol.15, pp.184-196, 1998.

9 H. Kumagai, H. Horie, H. Kuroiwa, H. Okamoto and S. Iwasaki, "Retrieval of cloud microphysics using 95-GHz cloud radar and microwave radiometer", Proc. SPIE, Vol. 4152, pp.364-371, 2000.

10 H. Okamoto, S. Iwasaki, M. Yasui, H. Horie, H. Kuroiwa and H. Kumagai, "An algorithm for retrieval of cloud microphysics using 95-GHz cloud radar and lidar", submitting Jornal Geo. Res. – Atomos., 2001.

11 D. Atlas, S. Y. Matrosov, A. J. Heymsfield, M-D Chou, and D. B. Wolf, "Radar and radiation properties of ice clouds", J. Appl. Meteor., Vol.34, pp. 2329-2345, Nov. 1995.

12 M. Yoshizaki, T. Kato, H. Eito, A. Adachi, M. Murakami, S. Hayashi and WMO-01 Observation Group, A report on "Winter MCSs (mesoscale convective systems) observations over the Japan Sea in January 2001 (WMO-01)" , Tenki, Vol.48, No.2, pp.33-43, 2001. (in Japanese)

HORIE Hiroaki

Senior Researcher, Cloud Profiling Radar Group, Applied Research and Standards Devision

Remote Sensing

OHNO Yuichi

Senior Researcher, Cloud Profiling Radar group, Applied Ressearch and Standards Division

Meteorology, Radar Remote Sensing

KUROIWA Hiroshi

Leader, Cloud Profiling Radar Group, Applied Research and Standards Division